**Natural Hazards
and Earth
System Sciences**

# Enhanced ULF radiation observed by DEMETER two months around the strong 2010 Haiti earthquake

**M. A. Athanasiou[1,2], G. C. Anagnostopoulos[3], A. C. Iliopoulos[3], G. P. Pavlos[3], and C. N. David[2]**

[1]Dept. of Information & Communications, Technical University of Serres, Greece
[2]Dept. of Mechanical Engineering, Technical University of Serres, Greece
[3]Dept. of Electrical & Computer Engineering, Democritus University of Thrace, Greece

**Abstract.** In this paper we study the energy of ULF electromagnetic waves that were recorded by the satellite DEMETER, during its passing over Haiti before and after a destructive earthquake. This earthquake occurred on 12 January 2010, at geographic Latitude 18.46° and Longitude 287.47°, with Magnitude 7.0 R. Specifically, we are focusing on the variations of energy of Ez-electric field component concerning a time period of 100 days before and 50 days after the strong earthquake. In order to study these variations, we have developed a novel method that can be divided in two stages: first we filter the signal, keeping only the ultra low frequencies and afterwards we eliminate its trend using techniques of Singular Spectrum Analysis (SSA), combined with a third-degree polynomial filter. As it is shown, a significant increase in energy is observed for the time interval of 30 days before the earthquake. This result clearly indicates that the change in the energy of ULF electromagnetic waves could be related to strong precursory earthquake phenomena. Moreover, changes in energy associated with strong aftershock activity were also observed 25 days after the earthquake. Finally, we present results concerning the comparison between changes in energy during night and day passes of the satellite over Haiti, which showed differences in the mean energy values, but similar results as far as the rate of the energy change is concerned.
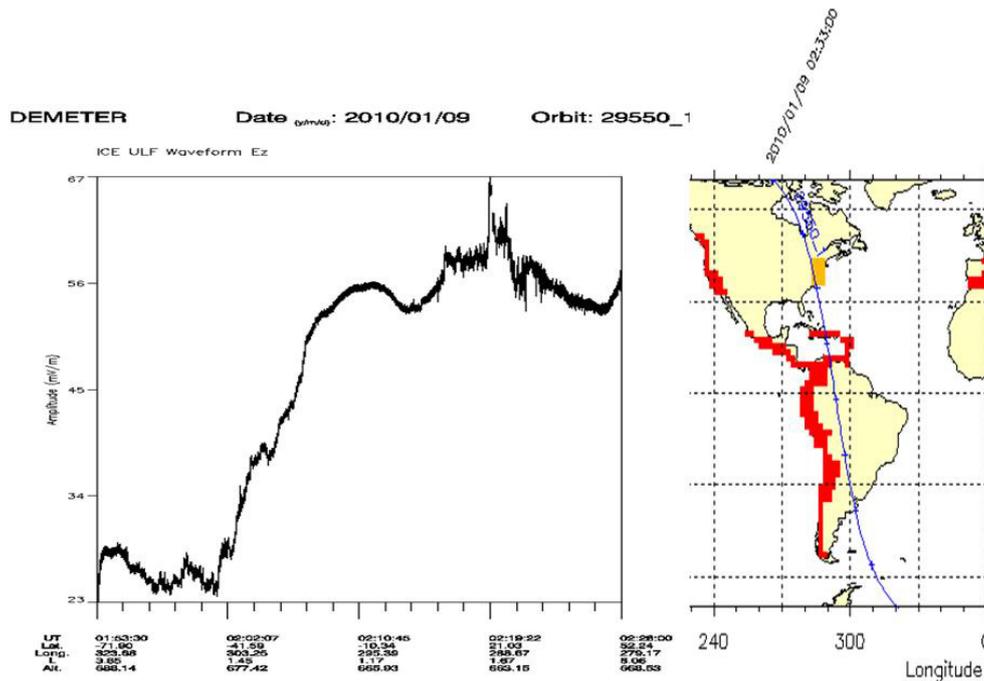
## 1 Introduction

Earthquakes (EQs) are complex phenomena generated by rock deformation in the brittle outer part of the Earth and are associated with large unpredictability, due to inherent extreme randomness (Kagan, 2007). However, in the last decades there is growing evidence that EQs precursory phenomena exist and can be detected. This evidence is based on studies of certain effects related to magnetic and telluric fields, ionospheric perturbations, nightglow observations and generation of electromagnetic (EM) emissions from DC to high frequency (HF) range and radiation belt precipitation in the upper ionosphere (Bhattacharya et al., 2007; Anagnostopoulos et al., 2010; Sidiropoulos et al., 2010). Theoretical studies and laboratory experiments suggest two main mechanisms for the production of precursor earthquake waves, namely the electromechanical mechanism and the acoustic mechanism. These mechanisms are mainly based on the deformation of rocks under pressure and temperature conditions existing in the brittle seismogenic crust which destabilise the mechanical and electrical properties of the solids. In particular, according to the electromechanical mechanism, electric charges are generated as the result of friction and piezoelectric phenomenon that change the Earth's electric field and generates EM waves, which are considered to propagate to the upper atmosphere and ionosphere (Lokner et al., 1983; Cress et al., 1987; Enomoto and Hashimoto, 1990; Parrot et al., 1993). On the other hand, according to the acoustic mechanism, gravity waves are generated before and after the earthquake. These waves propagate in the atmosphere where their amplitudes are increased relatively to height, due to the air's density decrease, disturb the ionosphere and cause VLF emissions of electromagnetic waves (Davies and Baker, 1965; Gokhberg et al., 1982; Ralchovski et al., 1985).

Most papers have been devoted to studies of ELF/VLF waves (Gokhberg et al., 1983; Larkina et al., 1983, 1989; Parrot and Lefeuvre, 1985; Parrot and Mogilevsky, 1989; Chmyrev et al., 1989; Serebryakova et al., 1992; Henderson et al., 1993; Zhang et al., 2009; Akhoondzadeh et al., 2010) and the analyses have been made mainly in the frequency domain (Fourier analysis), due to the large amount of data. However, Fourier analysis cannot capture some essential characteristics which are revealed in time domain analysis.

**Fig. 1.** The waveform of Ez electric field component (left) concerning the DEMETER's orbit 29550_1 (right) on 9 January 2010 for the time interval 01:53:30 – 02:26:00 UT. Moreover, on the x-axis of left image the values of Latitude, Longitude, L-value and Altitude of DEMETER are depicted.
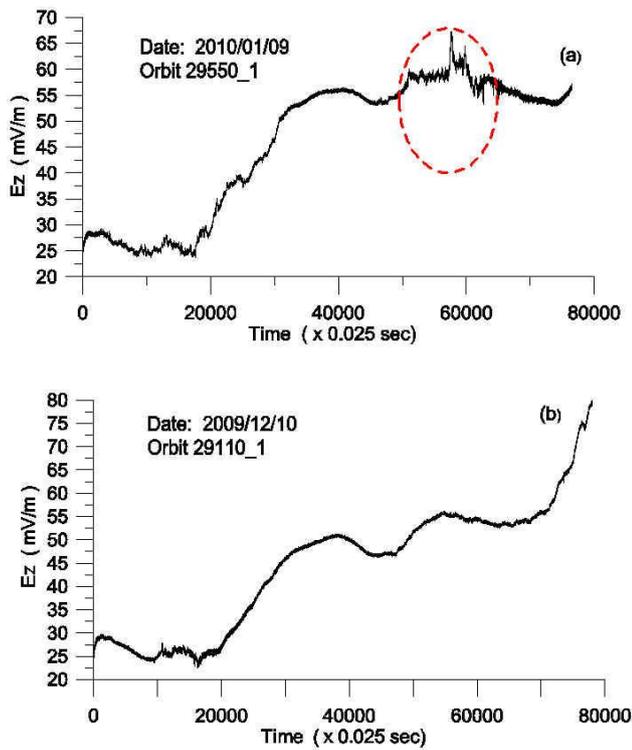
Moreover, there is growing evidence that the ionosphere is a strong nonlinear complex turbulent system (Blecki et al., 2010a, b; Unnikrishnan, 2010 and references therein). Thus, traditional Fourier analysis is not capable for analyzing signals related to significant nonlinear phenomena such as turbulence. The Fourier transform spreads information about localized features over all the scales making it impossible to study the evolution of different scale structures simultaneously. Nevertheless, recent studies with applications of the wavelet analysis and higher order spectra concerning electromagnetic disturbances over epicenter regions have been published (Blecki et al., 2010a, b), showing the presence of strong emissions in the ELF frequency domain in the Ionosphere 6 to 2 days or even 1 day before the earthquakes.

Here, we attempt a different investigation using ULF satellite EM signals observed in the upper ionosphere. Our methodology has the following advantages: (1) time domain analysis of EM ULF signals detected by a satellite in the upper ionosphere is a new tool in the related literature, (2) ELF/VLF waves compared to ULF waves weaken faster in the ionosphere, so a ULF study by a satellite in the upper ionosphere may have direct access to the EQ preparation zone, and therefore, may give more clear results concerning EQ preparation processes (Chmyrev et al., 1989), (3) There are, in general, a limited number of studies on the possible relation of ULF EM waves in the upper ionosphere with earthquakes (Fraser-Smith et al., 1990; Molchanov et al., 1992) (4) Even in studies concerning ELF/VLF emis-

sions (for example Henderson et al., 1993; Parrot, 1994), it was shown that significant EM emissions were also observed in ultra-low frequencies, namely 4–8 Hz and 4–16 Hz. (5) The amount of ULF data (much less than the corresponding ELF/VLF data) is suitable for analysis in the time domain as well as for the application of Singular Spectrum Analysis (6) Finally, significant emissions have been found in the range of $\sim$50 Hz (Blecki et al., 2010b), which are close to the range of the ULF scale (0–20 Hz). For these reasons, we chose to focus on space-based ULF EM emissions to study their energy changes during a long period before and after a strong EQ. Our study was based on the analysis of measurements from the DEMETER satellite around the deadly earthquake of Haiti on 12 January 2010.

## 2 Data analysis and results

For the estimation of ULF signals we used data derived from the DEMETER satellite database. Generally, the microsatellite DEMETER was launched on 29 June 2004, its orbit altitude was approximately 660 km and it took 14 orbits per day around the Earth. Among the Scientific Objectives of the DEMETER mission is the investigation of the Earth's Ionosphere and disturbances due to seismic and volcanic activities. The ICE instrument allows the measurements of the three components of the electromagnetic wave field from DC up to 3.5 MHz (Berthelier et al., 2006).
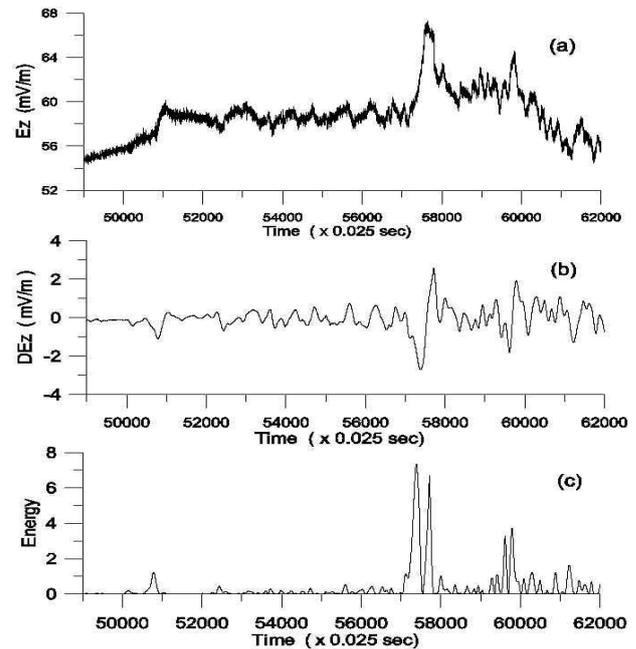
Fig. 2. Comparison of two different waveforms of the Ez electric field component, one (Fig. 2a) corresponding to the waveform presented in Fig. 1 and the other (Fig. 2b) corresponding to a time period where no earthquake occurred in the broad seismic region of Haiti.
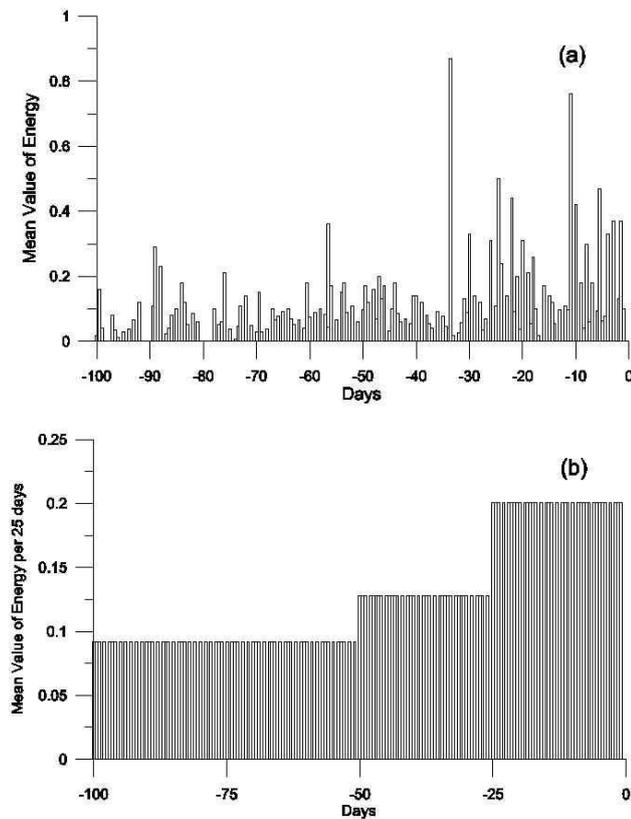


Fig. 3. (a) The perturbed waveform (shown in Fig. 2a) focussed on a time period between 49 000–62 000 (x 0.025 s). (b) The filtered, focused, perturbed signal (Fig. 3a). For filtering we used Singular Spectrum Analysis, combined with a third-degree polynomial filter. (c) The square power of the pre-Earthquake signal shown in Fig. 3b.

In this paragraph, we present results concerning the analysis of the z-component of electric field of the ULF waves, within the frequency range of 0–20 Hz. It should be noted that the analysis of the other components Ex, Ey, gives similar results (not shown in this paper). In particular, the data cover a time period of 150 days, 100 before and 50 after the earthquake, corresponding to 374 semi-orbits of the DEMETER satellite. These semi-orbits were carefully selected in order to be strongly related to the area where the earthquake took place. 207 of them correspond to night-passing (Up Orbits) over Haiti, while the rest correspond to day-passing (Down Orbits). The sampling frequency of data is 40 Hz, and the number of data per orbit is about 82 000.

Figure 1 shows the waveform of the electric field component Ez (left image) concerning the orbit 29550_1 (right image) on 9 January 2010 for the time interval 01:53:30 – 02:26:00 UT. Moreover, on the x-axis of the left image the values of Latitude, Longitude, L-value and Altitude of DEMETER are depicted. As it is shown within the red dashed line of Fig. 2a, there exists a significant fluctuation in the waveform, as the satellite passes over Haiti, in 02:16:00 – 02:23:00 UT and at 10°–30° Latitude.

Moreover, in Fig. 2 we present a comparison of two different waveforms of the Ez electric field component, one (Fig. 2a) corresponding to the waveform presented in Fig. 1 and the other (Fig. 2b), corresponding to a time period where no earthquake occurred in the broad seismic region of Haiti. From the observation of Fig. 2b, it is clear that there is no significant variation in the waveform corresponding to the period of seismic quiescence.

In order to estimate the energy of the possible pre-Earthquake signal, we focussed on the signal shown in Fig. 3a, which corresponds to the perturbed waveform (Fig. 2a). On this signal a low pass frequency filter was applied, keeping frequencies lower than 5 Hz, in order to estimate thoroughly the mean energy value. Consecutively, we used the methods of Singular Spectrum Analysis (Athanasiou and Pavlos, 2001) and polynomial fitting of third order in order to remove the signal trend that corresponds to exogenous factors. A brief description of Singular Spectrum Analysis is given in Appendix A. The resulting signal appears in the Fig. 3b. We consider that this waveform is the clear pre-Earthquake signal recorded by DEMETER satellite. The plot presented in Fig. 3c is the square power of the pre-Earthquake signal and consists of an estimation of its energy. In this case the mean value of energy was found to be 0.37 $(\mathrm{mV\,m})^{-2}$.
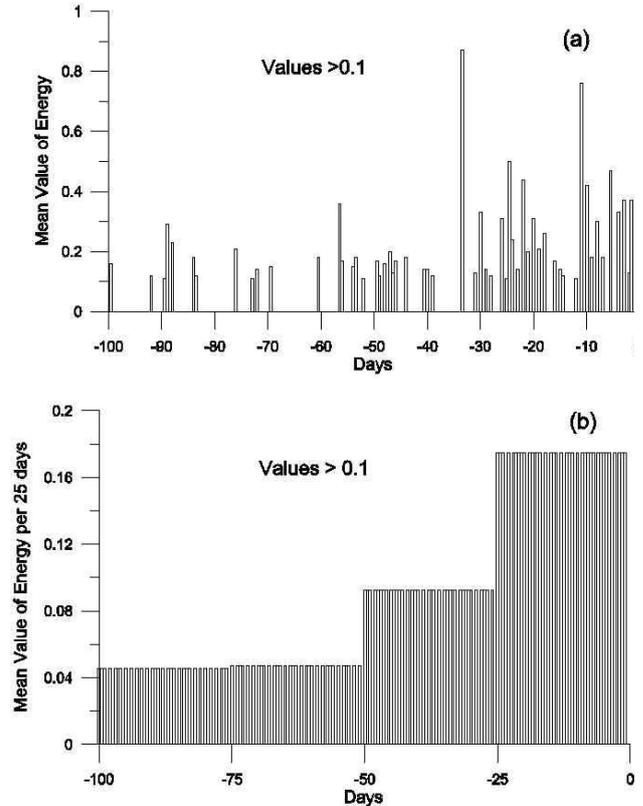
Figure 4a shows the mean value of energy for signals within the frequency range of 0–20 Hz, corresponding to the data of 135 perturbed and unperturbed semi-orbits which

**Fig. 4. (a)** The mean value of energy for signals corresponding to data recorded by the DEMETER satellite during its night-passing covering a time interval of 100 days before the strong Earthquake. As we can see in this figure, many significant increases in the mean value of the energy are observed in a time period of one month before the main Earthquake. **(b)** The mean value of energy of pre-earthquake signals per 25. The most significant change of energy is observed for the time interval 0–25 days before the earthquake.



**Fig. 5. (a)** Figure 5a is similar to Fig. 4a, but in this case we have rejected values smaller than 0.1 (mV m)$^{-2}$. As observed, most of the values of energy are concentrated in the time interval of one month before the earthquake. **(b)** Figure 5b is similar to Fig. 4b, but in this case we have replaced the values of energy greater than 0.1 (mV m)$^{-2}$ with zero. As it is shown in this figure, the most significant change of energy is observed for the time interval of 0–25 days before the earthquake.

cover a time interval of 100 days before the strong Earthquake, using the same procedure described previously in Fig. 3. These orbits were recorded by the DEMETER satellite during its night-passing (Up Orbits) over Haiti for the geographic Latitude 18.46 $\pm$ 10° (8°–28°) degrees and Longitude 287.47 $\pm$ 15° (272°–302°) degrees. This part of Earth can be considered as the seismic region around Haiti. Also in this seismic region and for this time interval, no earthquake with a magnitude greater than 5 took place. Thus, we assume that the observed signals can be related to precursor phenomena of the strong earthquake occurring 100 days later. As we can see in this figure, many significant increases in the mean value of the energy are observed in a time period of one month before the main Earthquake, while the first strong signal is detected 33 days before the event.
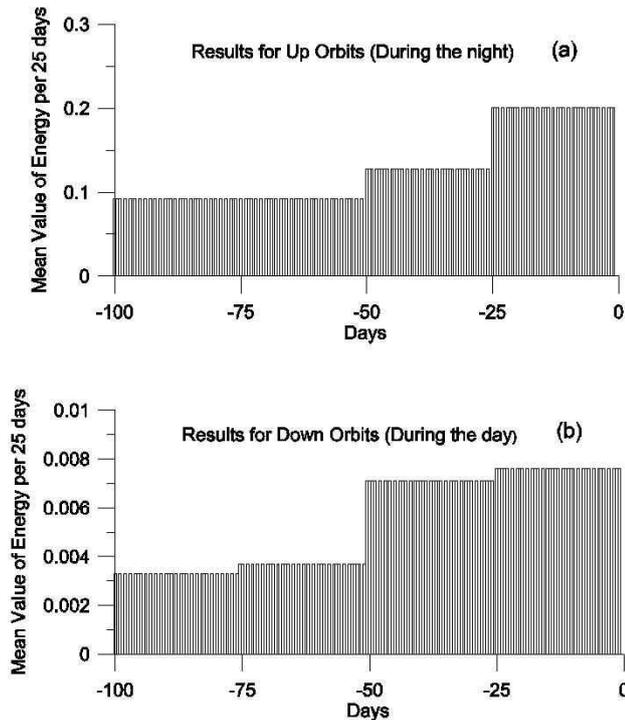
Figure 4b shows the estimation of the mean value of energy of pre-earthquake signals per 25 days. We observe that for the time interval 50–100 days before the main event, the

mean value of energy takes low values around 0.1 (mV m)$^{-2}$. The first significant change of energy is observed for the time interval of 25–50 days before the earthquake, where the mean value of energy is 0.13 (mV m)$^{-2}$, corresponding to an increase of 40%. Finally, the most significant change of energy is observed for the time interval 0–25 days before the earthquake, where the mean value of energy attains values around 0.21 (mV m)$^{-2}$, corresponding to an increase of 220%.

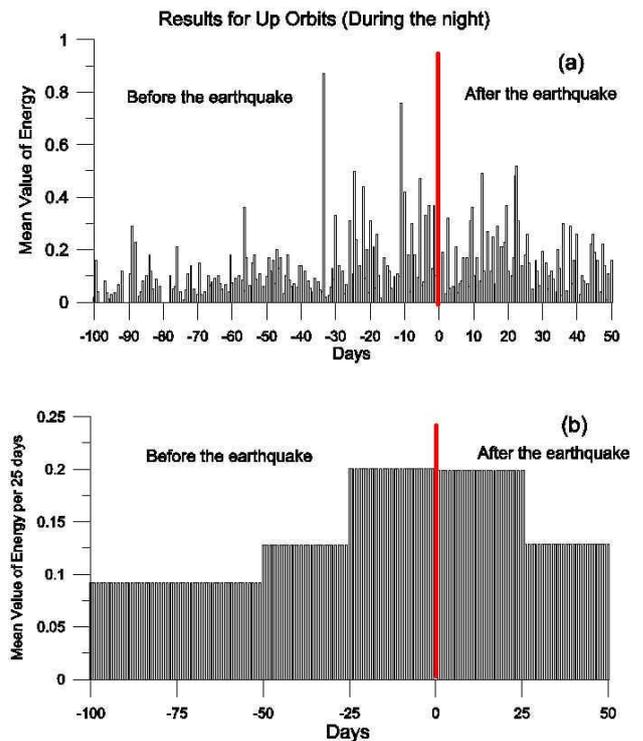Figure 5a is similar to Fig. 4a, but in this case we have rejected the values smaller than a threshold of 0.1 (mV m)$^{-2}$, which corresponds to the mean value of energy for the time interval 50–100 days before the earthquake, in order to further highlight the increases in the mean energy. As observed, most of the values of energy are concentrated in the time interval of one month before the earthquake. On the contrary, as far as the time interval 50–100 days before the earthquake is concerned, few and low-energy pre-earthquake signals are observed.

**Fig. 6.** Results of the mean value of energy per 25 days for the pre-earthquake signals recorded by the DEMETER satellite during night (**a**) and day passing (**b**) over Haiti. In both figures, the energy of the pre-earthquake signals increases at the same rate regarding the same time period before the earthquake.

**Fig. 7.** (**a**) The average energy of the pre-earthquake signals recorded by the satellite during night-passing for 100 days before the main earthquake as well as for the aftershock signals for 50 days. (**b**) The average energy per 25 days of the observed signal during the night, for 100 days before and 50 days after the earthquake.

Figure 5b is similar to Fig. 4b, but in this case, in order to estimate the mean value of energy per 25 days, we have replaced the values of energy that are greater than 0.1 $(mV\,m)^{-2}$ with zero, as is explained in the previous section. As it is shown in this figure, the mean value of energy obtains low values around 0.05 $(mV\,m)^{-2}$ for the time interval of 50–100 days before the earthquake. The first significant change of energy is observed for the time interval 25–50 days before the main event, where the mean value of energy is 0.1 $(mV\,m)^{-2}$, an increase of 100%. Finally, the most significant change of energy is observed for the time interval of 0–25 days before the earthquake, where the mean value of energy is 0.18 $(mV\,m)^{-2}$, corresponding to an increase of 360%.

Figure 6 presents results of the mean value of energy per 25 days for the pre-earthquake signals recorded by the DEMETER satellite during night (Fig. 6a) and day passing (Fig. 6b) over Haiti. Figure 6a is the same as Fig. 4b and has already been described. Figure 6b shows the mean value of energy for the signals recorded by DEMETER satellite during its day passing (Down Orbits) over Haiti for Latitude 18.46 ± 5° (13°–23°) degrees and Longitude 287.47 ± 15° (272°–302°) degrees. The data correspond to 131 semi-orbits covering a time interval of 100 days before the Earthquake.

The comparison of Fig. 6a, b shows that the energy perturbation of pre-seismic day-passing signals is much smaller than night-passing ones. As it was found for the time interval of 100 days before the earthquake, the mean value of energy during the day-passing was 0.005 $(mV\,m)^{-2}$ while for the night-passing it was 0.13 $(mV\,m)^{-2}$, namely 26 times greater. We think that this difference could be due to the strong ionization of the Ionosphere during daytime causing great attenuation in the pre-seismic signals. However, the results in Fig. 6a and b are very similar as far as the rate of energy change is concerned. In both figures, the energy of the pre-earthquake signals increases at the same rate regarding the time before the earthquake. This result indicates the efficiency of the applied method since it can reveal precursory phenomena in data concerning the day orbits, although the energy changes are very weak.

Figure 7a represents the average energy of the pre-earthquake signals recorded by the satellite during night-passing, for 100 days before the main earthquake as well as for the aftershock signals for 50 days. As we can see, there was a significant increase in the mean energy recorded a month before the main earthquake which remains at the same levels approximately for 25 days after, while consecutively

decreasing gradually. In Fig. 7b the overall picture of the energy change before and after the earthquake is shown. This figure shows the average energy per 25 days of the observed signal during the night, for 100 days before and 50 days after the earthquake. During the 70 days time interval after the main shock, 5 strong aftershocks of magnitude greater than 5, occurred in the broad seismogenic area of Haiti. We observe that the drop in the signal's mean energy during the first 25 days after the earthquake is insignificant. On the contrary, during the period of 25–50 days after the earthquake there is a significant reduction of 43% compared with the maximum value. One possible explanation for this reduction of mean energy after the earthquake is a respective decrease in seismic activity in the region of Haiti after the main earthquake.

# 3 Conclusions

In this study we have focussed on changes in the energy of electromagnetic ULF waves (0–20 Hz) of the electric field component Ez that were recorded by the satellite DEMETER, concerning a time period of 100 days before and 50 days after a strong earthquake which took place in Haiti in 12 January 2010. The analysis was based on a novel method consisted of two stages: first, the signals were filtered keeping only the very low frequencies, and consecutively their trend was eliminated by applying the techniques of Singular Spectrum Analysis combined with a third-degree polynomial filter. The results reveal a significant increase of the energy of ULF waves, up to 360%, for a period of one month before the strong earthquake compared to the energy of the background. Also, a gradual reduction of wave energy occurs one month after the main earthquake. Additionally, the comparison of pre-seismic day-passing and night-passing signals showed differences in the mean energy values, but similar results as far as the rate of energy change is concerned.

The results of this paper clearly indicate that ULF electromagnetic waves can be very useful in revealing possible precursor seismic phenomena in the Earth's Ionosphere. However, there is a possibility that similar results could be obtained due to a seasonal effect or other physical phenomena not related to seismogenesis. For example, Haiti is very close to the equator where equatorial electrojet can give a strong effect and ionospheric equatorial disturbances can also be very strong. Thus, the same analysis will be performed for the same days in which earthquakes occurred, but for a different year in order to exclude the possibility of seasonal or other physical effects. Finally, other strong earthquakes that occurred in low geographic latitudes will be studied using ULF waveforms in order to further establish the hypothesis of ULF seismo-electromagnetic precursory emission.

# Appendix A

## Singular Spectrum Analysis

In this appendix we give some practical details for the implementation of the methology presented in this paper. Singular Spectrum Analysis (SSA) has been proven to be a strong and effective method for modern time series analysis. It was used by Broomhead and King (1986) for the first time and originates from the generalized theory of information. Singular spectrum analysis is applied to the trajectory matrix constructed by an experimental time series as follows:

$$X = \begin{bmatrix} x(t_1), (t_1 + \tau), \dots x(t_1 + (n-1)\tau) \\ x(t_2), x(t_2 + \tau), \dots x(t_2 + (n-1)\tau) \\ \dots \\ x(t_N), x(t_N + \tau), \dots x(t_N + (n-1)\tau) \end{bmatrix} = \begin{bmatrix} x_1^T \\ x_2^T \\ . \\ x_N^T \end{bmatrix} \quad (A1)$$

where $x(t_i)$ is the observed time series and $\tau$ is the delay time for the phase space reconstruction. The rows of the trajectory matrix constitute the state vectors $x_i^T$ on the reconstructed trajectory in the embedding space $R^n$. As we have constructed $N$ state vectors in embedding space $R^n$ the problem is how to use them in order to find a set of linearly independent vectors in $R^n$ which can describe efficiently the attracting manifold within the phase space. These vectors constitute part of a complete orthonormal basis $\{e_i, i=1,2,\dots n\}$ in $R^n$ and can be constructed as a linear combination of vectors on the reconstructed trajectory in $R^n$ by using the relation

$$s_i^T X = \sigma_i c_i^T \quad (A2)$$

According to the Singular Value Decomposition (SVD) theorem it can be proved that the vectors $s_i$ and $c_i$ are eigenvectors of the structure matrix $XX^T$ and the covariance matrix $X^T X$ of the trajectory according to the relations

$$XX^T s_i = \sigma_i^2 s_i, \quad X^T X c_i = \sigma_i^2 c_i \quad (A3)$$

The vectors $s_i, c_i$ are the singular vectors of $X$ and $\sigma_i$ are its singular values, while the SVD analysis of $X$ can be written as

$$X = S \, \Sigma \, C^T \quad (A4)$$

where $S = [s_1, s_2, \dots s_n]$, $C = [c_1, c_2, \dots c_n]$ and $\Sigma = diag[\sigma_1, \sigma_2, \dots \sigma_n]$. The ordering $\sigma_1 \geq \sigma_2 \geq \dots \geq \sigma_n \geq 0$ is assumed. Moreover according to the SVD theorem the non-zero eigenvalues of the structure matrix are equal to non-zero eigenvalues of the covariance matrix. This means that if $n\prime$ (where $n\prime \leq n$) is the number of the nonzero eigenvalues, then rank $XX^T = \text{rank} X^T X = n\prime$. It is obvious that the $n\prime$–dimensional subspace of $R^N$ spanned by $\{s_i, i=1,2,\dots n\prime\}$ is mirrored to the basis vector $c_i$ which can be found as the linear combination of the delay vectors by using the eigenvectors $s_i$ according to Eq. (A2). The complementary subspace spanned by the set $\{s_i, i=n\prime+1,\dots N\}$ is mirrored to the origin of the

embedding space $R^n$ according to the same relation. That is, according to SVD analysis the number of the independent eigenvectors $c_i$ that are efficient for the description of the underlying dynamics is equal to the number $n'$ of the non-zero eigenvalues $\sigma_i$ of the trajectory matrix. The trajectory can be described in the new basis $\{c_i, i=1,2,\dots n\}$ by the trajectory matrix projected on the basis $\{c_i\}$ given by the product $XC$ of the old trajectory matrix and the matrix $C$ of the eigenvectors $\{c_i\}$. The new trajectory matrix $XC$ is described by the relation

$$(XC)^T(XC) = \Sigma^2 \tag{A5}$$

and its columns are called principal components. This relation corresponds to the diagonalization of the new covariance matrix so that in the basis $\{c_i\}$ the principal components of the trajectory are uncorrelated. Also, from the same relation Eq. (A5) we conclude that each eigenvalue $\sigma_i^2$ is the mean square projection of the trajectory on the corresponding $c_i$, so that the spectrum $\{\sigma_i^2\}$ includes information about the extending of the trajectory in the directions $c_i$ as it evolves in the reconstructed phase space. The explored by the trajectory phase space corresponds to the average to an $n$-dimensional ellipsoid for which $\{c_i\}$ give the directions and $\{\sigma_i\}$ the lengths of its principal axes. The replacement of the old trajectory matrix $X$ with the new $XC$ works as a linear filter for the entire trajectory. Moreover the SVD analysis permits to reconstruct (Elsner and Tsonis, 1996) the original trajectory matrix by using the $XC$ matrix as follows

$$X = \sum_{i=1}^{n} (Xc_i)c_i^T \tag{A6}$$

The part of the trajectory matrix which contains all the information about the deterministic trajectory, as it can be extracted by observations, corresponds to the reduced matrix

$$X_d = \sum_{i=1}^{n'} (Xc_i)c_i^T \tag{A7}$$

which is obtained by summing only for the eigenvectors $c_i$ with non-zero eigenvalues.

## References

Akhoondzadeh, M., Parrot, M., and Saradjian, M. R.: Investigation of VLF and HF waves showing seismo-ionospheric anomalies induced by the 29 September 2009 Samoa earthquake ($M_w$=8.1), Nat. Hazards Earth Syst. Sci., 10, 1061–1067, doi:10.5194/nhess-10-1061-2010, 2010.

Anagnostopoulos, G., Rigas, V., Atahanasiou, M., Iliopoulos, A., Vassiliadis, E., and Iossifidis, N.: Temporal Evolution of Energetic Electron Precipitation as a Promising Tool for Earthquake Prediction Research: Analysis of IDP/DEMETER observations, in: Advances in Hellenic Astronomy during the IYA09, ASP Conference Series, edited by: Tsinganos, K., Hatzidimitriou, D., and Matsakos, T., 424, 67–74, 2010.

Athanasiu, M. A. and Pavlos, G. P.: SVD analysis of the magnetospheric AE index time series and comparison with low-dimensional chaotic dynamics, Nonlin. Processes Geophys., 8, 95–125, doi:10.5194/npg-8-95-2001, 2001.

Berthelier, J. J., Godefroy, M., Leblanc, F., Malingre, M., Menvielle, M., Lagoutte, D., Brochot, J. Y., Colin, F., Elie, F., Legendre, C., Zamora, P., Benoist, D., Chapuis, Y., and Artru, J.: ICE, The electric field experiment on DEMETER, Planet. Space Sci., 54, 5, 456–471, 2006.

Bhattacharya, S., Sarkar, S., Gwal, A. K., and Parrot, M.: Satellite and ground-based ULF/ELF emissions observed before Gujarat earthquake in March 2006, Curr. Sci. India, 93(1), 41–46, 2007.

Blecki, J., Parrot, M., and Wronowski, R.: Plasma turbulence in the ionosphere prior to earthquakes, some remarks on the DEMETER registrations, JAES, doi:10.1016/j.jseaes.2010.05.016, 2010a.

Blecki, J., Parrot, M., and Wronowski, R.: Studies of the electromagnetic field variations in ELF frequency range registered by Demeter over the Sichuan region prior to the 12 may 2008 earthquake, IJRS, doi:10.1080/01431161003727754, 2010b.

Broomhead, D. S. and King, G. P.: Extracting qualitive dynamics from experimental data, Physica D 20, 217–236, 1986.

Chmyrev, V. M., Isaev, N. V., Bilichenko, S. V., and Stanev, G.: Observation by space – borne detectors of electric field and hydrodynamics waves in the ionosphere over an earthquake centre, Phys. Earth Planet Inter., 57, 110–114, 1989.

Cress, O. O., Brady, B. T., and Rowell, G. A.: Source of electromagnetic radiation from fractures of rock samples in the laboratory, Geophys. Res. Lett., 14, 331, 1987.

Davies, K. and Baker, D. M.: Ionospheric effects observed around the time of the Alaskan earthquake of March 28, 1964, J. Geophys. Res., 70, 2251–2263, 1965.

Elsner, J. B. and Tsonis, A. A.: Singular Spectrum Analysis: A new tool in time series analysis, Plenum Press, New York, 1996.

Enomoto, Y. and Hashimoto, H.: Emission of charged particles 199 from indentation fracture of rocks, Nature, 346, 641, 1990.

Fraser-Smith, A. C., Bernardi, A., McGill, P. R., Ladd, M. E., Helliwell, R. A., and Villard Jr., O. G.: Low – frequency magnetic field measurements near the epicenter of the M 7.1 Loma Prieta earthquake, Geophys. Res. Lett., 17, 1465, 1990.

Gokhberg, M. B., Morgounov, V. A., Yoshimo, T., and Tomizawa, I.: Experimental measurement of electromagnetic emission possibly related to earthquakes in Japan, J. Geophys. Res., 87, 7824–7828, 1982.

Gokhberg, M. B., Pilipenko, V. A., and Pokhotelov, O. A.: Satellite observation of electromagnetic radiation over the epicentral

region of an incipient earthquake, Dokl. Akad. Nauk. SSSR Earth Sci. Ser., Engl. Transl., 268(1), 5–7, 1983.

Henderson, T. R., Sonwalker, V. S., Helliwell, R. A., Inan, U. S., and Fraser-Smith, C.: A search for ELF/VLF emissions induced by earthquakes as observed in the ionosphere by the DE-2 satellite, J. Geophys. Res., 98, 9503–9514, 1993.

Kagan, Y. Y.: Why does theoretical physics fail to explain and predict earthquake occurrence?, Lect. Notes Phys., 705, 303–359, 2007.

Larkina, V. I., Nalivaiko A. V., Gershenson N. I., Gohkberg, M. B., Liperovsky, V. A., and Shalimov, S. L.: Observations of VLF emission related with seismic activity on the satellite INTERCOSMOS-19, Geomagn. Aeronomy, 23(5), 684–687, 1983.

Larkina, V. I., Migulin, V. V., Molchanov, O. A., Kharkov, I. P., Inchin, A. S., and Schvetcova, V. B.: Some statistical results on very low frequency radiowave emissions in the upper ionosphere over earthquake zones, Phys. Earth Planet. Inter., 57, 100 –109, 1989.

Lokner, D. A., Johnston, M. J. S., and Byerlee, J. D.: A mechanism to explain the generation of earthquake lights, Nature, 302, 28, 1983.

Molchanov, O. A., Kopytenko, Y. A., Voronov, P. V., Kopytenko, E. A., Matiashvilli, T., Fraser-Smith, A. C., and Bernardi, A.: Results of ULF magnetic field measurements near the epicenters of the Spitak (M=6.9) and Loma Prieta (M=7.1) earthquakes: Comparative analysis, Geophys. Res. Lett., 1, 9, 1495–1498, 1992.

Parrot, M. and Lefeuvre, F.: Correlation between GEOS VLF emissions and earthquakes, Ann. Geophys., 3, 737–748, 1985, http://www.ann-geophys.net/3/737/1985/.

Parrot, M. and Mogilevsky, M. M.: VLF emissions associated with earthquakes and observed in the ionosphere and the magnetosphere, Phys. Earth Planet Inter., 57, 86–99, 1989.

Parrot, M., Achache, J., Berthelier, J. J., Blanc, E., Deschamps, A., Lefeuvre, F., Menvielle, M., Planet, J. L., Tarits, P., and Villain, J. P.: High frequency seismo-electromagnetic effects, Phys. Earth Planet. Inter., 77, 65, 1993.

Parrot, M.: Seismo-Electromagnetic Waves Detected by Low-Altitude Satellites, in: Electromagnetic Phenomena Related to Earthquake Prediction, edited by: Hayakawa, M. and Fujinawa, Y., 361–272, Terra Sci. Publis. Company, Tokyo, 1994.

Ralchovski, T. M. and Christolov, L. V.: On low-frequency radio emission during earthquakes, C.R. Acad. Bulg. Sci., 38, 863–865, 1985.

Serebryakova, O. N., Bilichenko, S. V., Chmyrev, V. M., Parrot, M., Rauch, J. I., Lefeuvre, F., and Pokhotelov, O. A.: Electromagnetic ELF radiation from earthquake regions observed by low-altitude satellites, Geophys. Res. Lett., 19, 91–94, 1992.

Sidiropoulos, N., Anagnostopoulos, G., and Rigas, V.: Radiation belt electron precipitation in the upper ionosphere (700 km): Earthquake induced or ground transmitter stimulated?, Proccedings of 15th Conference Microwave Techniques, COMITE 2010, Brno, Czech Republic, 161–164, 19–21 April 2010.

Unnikrishnan, K.: A comparative study on chaoticity of equatorial/low latitude ionosphere over Indian subcontinent during geomagnetically quiet and disturbed periods, Nonlin. Processes Geophys., 17, 765–776, doi:10.5194/npg-17-765-2010, 2010.

Zhang, X., Qian, J., Ouyang, X., Shen, X., Cai, J., and Zhao, S.: Ionospheric electromagnetic perturbations observed on DEMETER satellite before Chile M7.9 earthquake, Earth. Sci., 22, 251–255, 2009.